Two-dimensional acoustic anisotropic (VTI) full waveform inversion: the Valhall case study

Y. Gholami[1], *R. Brossier*[2], *S. Operto*[1], *V. Prieux*[1], *A. Ribodetti*[1] *and J. Virieux*[2]
[1] *Géoazur - CNRS - University Nice Sophia-Antipolis;* [2] *ISTerre - University Joseph Fourier*

SUMMARY

Anisotropy can have a significant footprint in seismic imaging from surface wide-aperture data, because of the difference between vertical and horizontal velocities in vertical transversely isotropic (VTI) media. A key issue in anisotropic full waveform inversion (FWI) is to define a suitable parametrization of the subsurface model, and the number of parameter classes that can be reliably reconstructed for the chosen parametrization. We address this issue with an application of frequency-domain acoustic isotropic/anisotropic FWI to real surface wide-aperture data recorded by an ocean bottom cable in the Valhall field. Isotropic FWI results show that the horizontal velocity is mainly reconstructed in the upper structure, dominantly constrained by diving waves and supercritical reflections. This can lead to depth stretching and/or overestimated velocity perturbations in the deep velocity structure, mainly controlled by short-aperture reflections. Mono-parameter anisotropic FWI shows a reliable reconstruction of either the vertical, the horizontal or the NMO velocity, when the model is parametrized by one wave speed and the Thomsen's parameters δ and ε. For such mono-parameter FWI, the smooth δ and ε background models are kept constant during FWI iterations. Alternatively, the vertical and the horizontal velocities can be jointly reconstructed by multiparameter FWI, when the subsurface model is parametrized by the two wave speeds and δ, this latter is kept fixed during FWI iterations.

INTRODUCTION

Full Waveform inversion (FWI) is a multiscale data-fitting approach for high-resolution velocity model building from wide-aperture / wide-azimuth acquisition geometries (see Virieux and Operto (2009) for a review). Inversion of a broad range of aperture angles in the data allows one to image a continuous broadband of wavelengths in the medium, hence, leading to high-resolution models of the subsurface (e.g., Pratt and Worthington, 1990; Pratt, 1999; Sirgue and Pratt, 2004). Wide-aperture / wide-azimuth acquisition geometries increase, however, the potential footprint of anisotropy in seismic imaging, because of the intrinsic difference between vertical and horizontal velocities in vertical transversely isotropic (VTI) media (Pratt and Sams, 1996). It is therefore necessary to involve anisotropy in FWI of surface wide aperture data. In the 2D acoustic approximation, a VTI medium is described by 3 classes of anisotropic parameters (i.e., without considering density and attenuation). One example of such parametrization involves V_{P_0},δ, ε, where V_{P_0} is the vertical velocity and δ and ε are the Thomsen's parameters (Thomsen, 1986). Two other possible parametrization involve V_{P_0}, V_h, δ and V_{NMO}, V_h, δ, where $V_{NMO} = V_{P_0}\sqrt{1+2\delta}$ and $V_h = V_{P_0}\sqrt{1+2\varepsilon}$ are the normal-move-out (NMO) and the horizontal velocities, respectively. A first critical issue in multiparameter FWI is to define the most reliable parametrization (see Tarantola (1986) and Forgues and Lambaré (1997) for a discussion on the parametrization of acoustic and elastic inversions of seismic reflection data). A second issue is to define the number of parameter classes within the chosen parametrization which can be reliably reconstructed. The criteria to choose the parametrization and the number of inverted parameter classes are related to the sensitivity of the data to each parameter class and the potential trade-off between different parameter classes with respect to the aperture angle. A theoretical analysis of the parametrization of the 2D acoustic VTI FWI based on the eigenvalue/eigenvector decomposition of the Hessian has been performed by Plessix and Cao (2011), who show that V_{NMO} and V_h can be reliably reconstructed from long offset data. Gholami et al. (2010) and Gholami et al. (2011) present an analysis of the radiation pattern of the anisotropic parameters (i.e., the radiation pattern of the virtual point sources from which partial derivative of the data with respect to model parameters are computed, (Pratt et al., 1998)) as well as a grid search analysis of the misfit function for canonical models to influence of the different parameter classes in the data. These studies show that the seismic data are significantly more sensitive to the wave speeds (either V_{P_0}, V_h or V_{NMO}) relative to the Thomsen's parameters δ and ε. This implies that only the wave speed can be reconstructed when the chosen parametrization involves one wave speed and the Thomsen's parameters. In contrast, the sensitivity of the data to V_{P_0} and V_h is of the same order of magnitude. Moreover, these two parameters should be reasonably uncoupled because their radiation patterns are significantly different. Therefore, the joint reconstruction of the two wave speeds should be feasible, although the spatial resolution of the imaging of the two parameters can be different.

In this study, we validate the above-mentioned statements against an application of 2D acoustic isotropic and anisotropic (VTI) FWI to a real wide-aperture ocean-bottom-cable (OBC) data set from the Valhall field, where the presence of significant anisotropy is acknowledged. We first discuss the real meaning of the velocity reconstructed by isotropic FWI of anisotropic wide-aperture data. Then, we show the results of the mono-parameter and multi-parameter anisotropic FWI, for which different model-space parametrization are used.

METHOD

We apply 2D visco-acoustic VTI frequency-domain FWI using an extension to VTI media of the isotropic visco-elastic code of Brossier (2011). Seismic modeling is performed with a frequency-domain velocity-stress discontinuous Galerkin method for VTI medium parametrized by the elastic moduli c_{11}, c_{33}, c_{13}, and c_{44} and the density ρ. In the acoustic approximation, the shear wavespeed on the symmetry axis is set to zero. The

inversion is performed with a preconditioned steepest-descent method. The gradient of the misfit function is preconditioned by a 2D Gaussian filtering to remove high wavenumber artifacts and by the diagonal terms of the approximate Hessian to compensate for geometrical spreading (e.g., Ravaut et al., 2004). The gradient of the misfit function C with respect to model parameter $m_{i,j}$ is computed with the adjoint state method (Plessix, 2006) and is given by

$$\nabla C_{m_{i,j}} = -\Re\left\{ \mathbf{p}^T \frac{\partial \mathbf{A}^T}{\partial m_{i,j}} \overline{\lambda} \right\}, \quad (1)$$

where the real part of a complex number is denoted by $\Re$, the conjugate of a complex number by the sign $^-$, the incident pressure wavefield by $\mathbf{p}$ and the so-called back-propagated adjoint wavefield by λ. The forward problem operator in the frequency domain is denoted by $\mathbf{A}$. In equation 1, the gradient is given for one frequency and one source. The gradient corresponding to multiple sources and frequencies is computed by summation of the elementary gradients associated with each source-frequency couple. The index i of the model parameter $m_{i,j}$ denotes the spatial position of the parameter $m_{i,j}$ in the discretized model, while the index j denotes one parameter class in the parametrization of the model. The matrix $\frac{\partial \mathbf{A}}{\partial m_{i,j}}$ provides some insights on the sensitivity of the data to the parameter class j as a function of the aperture angle. This matrix describes the radiation pattern of the virtual source of the partial derivative of the wavefield with respect to the model parameter $m_{i,j}$ (Pratt et al., 1998). Note that the radiation pattern associated with a given parameter class j (for example, the horizontal velocity) can vary significantly depending on the chosen parametrization. Therefore, the choice of the model parametrization is a key issue in FWI, because the radiation pattern controls the spatial resolution of the imaging as well as the potential trade-off between different parameter classes.

APPLICATION TO REAL DATA

We present an application of 2D visco-acoustic isotropic and anisotropic (VTI) FWI to the hydrophone component of an ocean bottom cable data set recorded in the Valhall field. The shallow-water Valhall oilfield in the North Sea is characterized by a gas cloud, which hampers the imaging of reflectors at the oil reservoir level at 2.5-km depth, and by a significant VTI anisotropy with a vertical velocity 15% slower than the horizontal velocity (Kommedal et al., 2004). In this study, we consider the cable 21 of the 3D data set, that has been previoulsy processed by 3D isotropic acoustic FWI (Sirgue et al., 2010). This line is located at the end of the gas cloud. The shot and receiver spacing is 50 m, and the maximum offset in the acquisition is 13 km. A receiver gather for the hydrophone component is shown in Fig. 1a. First arrivals and the reflections from top and bottom of the gas layers are highlighted in the seismograms. Comparison between recorded seismograms and synthetic seismograms, computed in an isotropic NMO velocity model built by reflection traveltime tomography (Fig. 1(b-c)), shows a significant delay of the modeled first-arrival traveltimes. The isotropic NMO velocity model was updated by first-arrival traveltime tomography (FATT), leading to higher velocity in the first 1.5 km of the medium (Fig. 1(d)). Seismograms computed in the FATT model shows an improved agreement of the first arrivals at the expense of that of the reflected waves (Fig. 1(e)). These modelings highlight the footprint of the anisotropy in the data: the early-arriving phases, which propagates only in the upper structure due to insufficient long-offset coverage, are mainly controlled by the horizontal velocity, while the short-aperture reflections from the top and the base of the gas layers are mainly controlled by the NMO velocity.

Isotropic FWI

We first apply isotropic FWI to the OBC data set (Prieux et al., 2010). We successively invert 5 frequency groups: [3.5, 3.78, 4], [4, 4.3, 4.76], [4.76, 5, 5.25], [5.25, 5.6, 6] and [6, 6.35, 6.7] Hz with 25 iterations per frequency groups. The initial model for FWI is the isotropic NMO velocity model (Fig. 1b), that has been inferred from the V_{P_0} and δ models developed by anisotropic reflection traveltime tomography (Fig. 2(a)-(c)). The density model is inferred from the initial V_{P_0} model using the Gardner law (Gardner et al., 1974). A homogeneous attenuation model was defined by trial-and-error such that the root-mean squares amplitudes of the early-arriving phases computed in the initial model roughly matches that of the recorded data. We found 150 for the best fitting attenuation factor Q_P. Both the density and the attenuation models are kept fixed during FWI iterations. The final isotropic FWI velocity model is shown in Fig. 3a. The model shows a shallow reflector at 500-m depth and a series of low-velocity gas layers between 1.5 and 2.5 km depth. Some reflectors below the reservoir level can be interpreted and can be compared with that shown in Sirgue et al. (2010,their figure 3b). Confrontation of the FWI velocity model with the vertical velocities measured in a well shows that the horizontal velocity is reconstructed in the upper structure mainly constrained by the wide-aperture components of the data (Left panel of Fig. 3e). No obvious evidence of depth stretching of the deep velocity structure is shown for the particular starting velocity model and the data preconditioning we use. However, we notice overestimated low-velocity perturbations in the gas layers which can have been artificially created to balance the high horizontal velocities in the upper structure (Left panel of Fig. 3e). This kinematic balance is required to match the deep short-aperture reflections from the top of the reservoir level. Synthetic seismograms computed in the final isotropic FWI model shows a good agreement with the observed seismograms (Fig. 4), that highlights the ill-posedeness of the FWI of the anisotropic data in terms of non unicity of the solution. The improvement in the match between recorded and modeled seismograms after FWI can be assessed by comparing Figures 1c and 4.

Mono-parameter anisotropic FWI

The sensitivity analysis of acoustic anisotropic FWI has shown that the data are more sensitive to wave speed perturbations (i.e., V_{P_0}, V_h, or V_{NMO}) relative to Thomsen's parameter perturbations (Gholami et al., 2011). Therefore, the model space should be parametrized by one wave speed and the Thomsen's parameters when one seeks to reconstruct one single parameter, keeping the δ and ε parameter constant over FWI iterations. Moreover, the radiation pattern of the velocity parame-

ter is isotropic when the parametrization combines one wave speed with the Thomsen's parameters (Gholami et al., 2011). Therefore, a good spatial resolution of the velocity parameter is expected when such parametrization is used. This is confirmed by the results of mono-parameter FWI for V_{P_0}, V_h, and V_{NMO}, respectively (Fig. 3(b-d)). The initial models for FWI are shown in Fig. 2. The three FWI velocity models (V_{P_0}, V_h, and V_{NMO}) are of comparable quality and resolution. Confrontation of the FWI vertical velocity model with the well log shows a good agreement between the measured and the reconstructed vertical velocity (Fig. 3e). The horizontal and the NMO velocities reconstructed by FWI remain centered on the corresponding initial models, suggesting a stable reconstruction of these two parameters.

Multi-parameter anisotropic FWI

The parametrization analysis of the anisotropic FWI presented in Plessix and Cao (2011) and Gholami et al. (2011) suggests that the sensitivity of V_{P_0} and V_h is of the same order of magnitude and that the radiation pattern of the two wavespeeds do not overlap significantly. Therefore, the joint reconstruction of both parameters should be possible. We consider the parametrization (V_{P_0}, V_h,δ) for the model space, where δ is kept constant over FWI iterations. The initial V_{P_0}, V_h and δ models for FWI are shown in Fig. 2(a-c). The final FWI models for V_{P_0} and V_h are shown in Fig. 5(a-b) and suggest a reliable reconstruction of the two wave speeds. The spatial resolution of the V_{P_0} model (Fig. 5a) is comparable to that obtained by mono-parameter FWI (Fig. 3b), while the resolution of the V_h model (Fig. 5b) is significantly degraded relative to that obtained by mono-parameter FWI (Fig. 3c). This is consistent with the radiation patterns of the V_h parameter for the parametrization $(V_h, \delta, \varepsilon)$ and (V_{P_0}, V_h, δ) (Gholami et al., 2011). The spatial resolution of the FWI V_h model (Fig. 5b) has however been improved relative to that of the initial V_h model (Fig. 2b). We also performed the FWI for the joint reconstruction of V_{P_0} and ε, keeping δ constant over FWI iterations (not shown here). This leads to a V_{P_0} model which is close to the models shown in Figs. 3b and 5a. However, the FWI failed to update significantly the ε model because of the limited sensitivity of the data to ε.

CONCLUSION

We have presented an application of acoustic isotropic and anisotropic FWI to real surface wide-aperture data from the Valhall field, where the presence of significant VTI anisotropy is acknowledged. We have shown that isotropic FWI reconstructs the horizontal velocity in the upper structure, mainly controlled by the wide aperture components of the data. This can lead to depth stretching and/or overestimated velocity perturbations in the deep velocity structure, mainly controlled by short-aperture reflections. Although these bias in the velocity reconstruction, a good match of the wide aperture data has been achieved by full waveform seismic modeling, hence, highlighting the intrinsic ill-posedness of the anisotropic FWI. Mono-parameter anisotropic FWI can provide reliable FWI velocity models for either the vertical velocity, the horizontal velocity or the NMO velocity, when the model space is parametrized by one wave speed and the Thomsen's parameters δ and ε. The δ and ε background models are kept constant over FWI iterations and should describe sufficiently accurately the long-wavelength variations of the medium. Alternatively, two wave speed parameters (for example, the vertical and horizontal velocities) can be jointly reconstructed when the model space is parametrized by the two wave speeds and δ. In this case too, the δ background model is kept constant over FWI iterations. Further work is required to define more precisely the accuracy needed in the initial anisotropic models and to implement useful a priori constraints on anisotropy in FWI.

ACKNOWLEDGMENTS

This study has been funded by the SEISCOPE consortium http://seiscope.oca.eu, sponsored by BP, CGG-VERITAS, ENI, EXXON-MOBIL, SAUDI ARAMCO,SHELL, STATOIL and TOTAL. Computations have been done on the 'Mesocentre SIGAMM', hosted by Observatoire de la Cote d'Azur. This work was granted access to the HPC ressources of CINES / IDRIS under the allocation (project gao2280) made by GENCI (Grand Equipement National de Calcul Intensif). We thank BP Norge and Hess Norge for providing us the Valhall data and the initial models, and O. I.Barkved (BP Norge AS) and J. H. Kommedal (BP Norge AS) for fruitfull discussions.

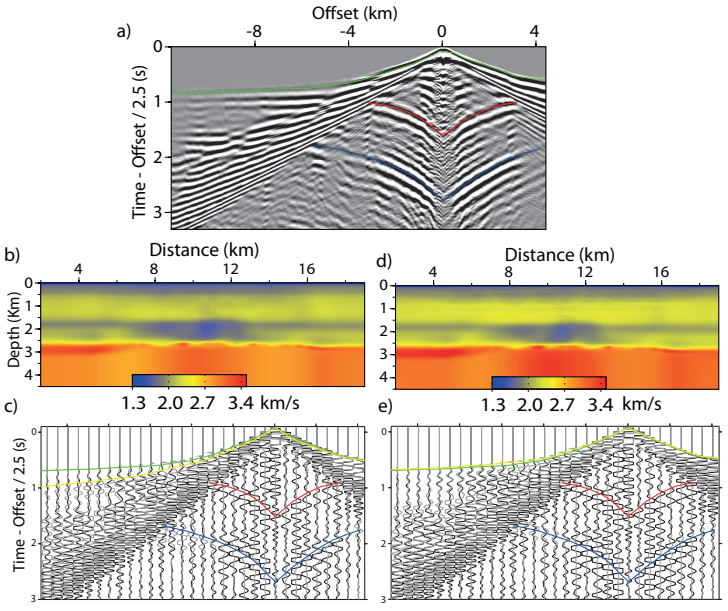

Figure 1: Isotropic seismic modeling. (a) Recorded receiver gather plotted with a reduction velocity of 2.5 km/s. The first arrivals and the reflections from the top and the bottom of the gas layers are highlighted with green, red and blue curves, respectively. (b) NMO velocity model, inferred from the V_{P_0} and the δ models shown in Fig. 2(a)-(c). (c) Direct comparison between recorded seismograms (black) and synthetic seismograms computed in the NMO velocity model shown in (a). (d) As (b) after velocity model update by FATT. (e) As (c) for synthetic seismograms computed in the FATT model (d).

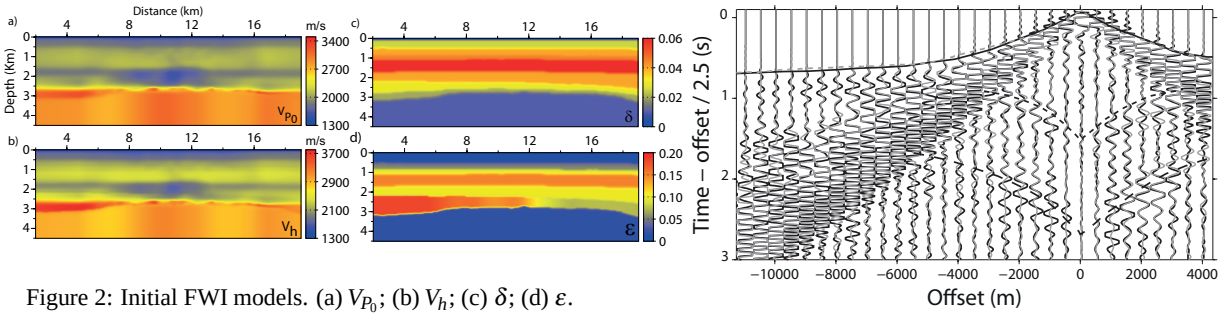

Figure 2: Initial FWI models. (a) V_{P_0}; (b) V_h; (c) δ; (d) ε.

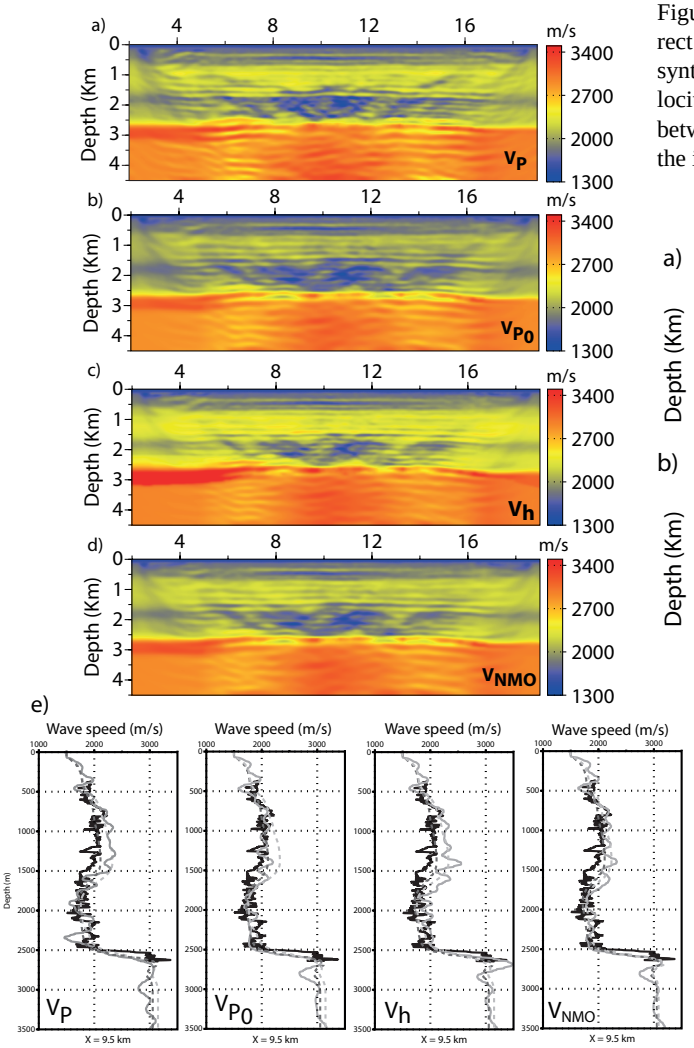

Figure 3: Final models of mono-parameter FWI. (a) isotropic V_P FWI model. (b) V_{P_0} FWI model. (c) V_h FWI model. (d) V_{NMO} FWI model. In (b-d), the model space is parametrized by one wave speed ((b) V_{P_0}, (c) V_h, (d) V_{NMO}) and the Thomsen's parameters δ and ε, these latter are kept constants over FWI iterations. (e) Comparison between the well log for vertical velocities (black line) and the corresponding log of the FWI models(solid gray curve). The black and gray dash curves are the initial V_{P_0} and V_h models, respectively, except on the right panel where the V_{NMO} profile is plotted instead of the V_h one.

Figure 4: Seismic modeling in the isotropic FWI model. Direct comparison between recorded seismograms (black) and synthetic seismograms computed in the final isotropic FWI velocity model shown in Fig. 3(a). Note the good agreement between the recorded and the modeled seismograms, although the isotropic approximation is used in the modeling.

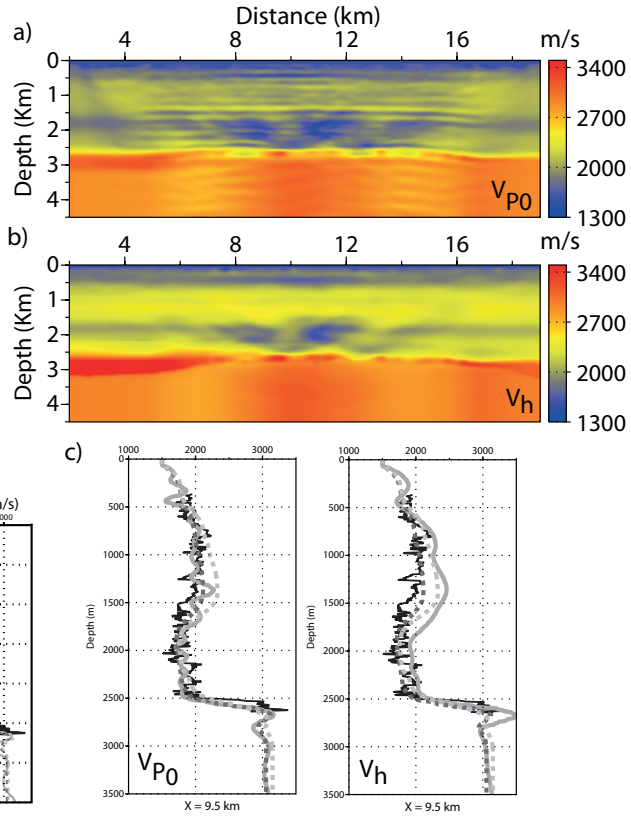

Figure 5: Final models of multi-parameter FWI. The model space is parametrized by V_{P_0}, V_h and δ. V_{P_0} and V_h are jointly reconstructed by FWI, while δ is kept constant over FWI iterations. The initial models are shown in Fig. 2(a-b)-(c). (a) V_{P_0} FWI model. (b) V_h FWI model. Note the more limited resolution of V_h relative to V_{P_0}. (c) Comparison between the well log for vertical velocities (black line) and the corresponding log of the FWI models (solid gray curve). From left to right, the log of the V_{P_0} and V_h FWI models are plotted. The black and gray dash curves are the initial V_{P_0} and V_h models, respectively.

EDITED REFERENCES

Note: This reference list is a copy-edited version of the reference list submitted by the author. Reference lists for the 2011 SEG Technical Program Expanded Abstracts have been copy edited so that references provided with the online metadata for each paper will achieve a high degree of linking to cited sources that appear on the Web.

REFERENCES

Brossier, R., 2011, Two-dimensional frequency-domain visco-elastic full-waveform inversion: parallel algorithms, optimization and performances: Computers & Geosciences, **37**, no. 4, 444–455, doi:10.1016/j.cageo.2010.09.013.

Forgues, E., and G. Lambar'e, 1997, Parameterization study for acoustic and elastic rayborn inversion: Journal of Seismic Exploration, **6**, 253–278.

Gardner, G. H. F., L. W. Gardner, and A. R. Gregory, 1974, Formation velocity and density — The diagnostic basics for stratigraphic traps: Geophysics, **39**, 770–780, doi:10.1190/1.1440465.

Gholami, Y., R. Brossier, S. Operto, V. Prieux, A. Ribodetti, and J. Virieux, 2011, Acoustic VTI full waveform inversion: sensitivity analysis and realistic synthetic examples: Presented at the 81st Annual International Meeting, SEG.

Gholami, Y., A. Ribodetti, R. Brossier, S. Operto, and J. Virieux, 2010, Sensitivity analysis of full waveform inversion in VTI media: 72nd Annual International conference and Exhibition, EAGE, Extended Abstracts, 8192.

Kommedal, J. H., O. I. Barkved, and D. J. Howe, 2004, Initial experience operating a permanent 4C seabed array for reservoir monitoring at Valhall: 74th Annual International Meeting, SEG, Expanded Abstracts, **23**, 2239–2242, doi:10.1190/1.1839696.

Plessix, R.-E., 2006, A review of the adjoint-state method for computing the gradient of a functional with geophysical applications: Geophysical Journal International, **167**, no. 2, 495–503, doi:10.1111/j.1365-246X.2006.02978.x.

Plessix, R. E. and Q. Cao, 2011, A parametrization study for surface seismic full waveform inversion in an acoustic vertical transversely isotropic medium: Geophysical Journal International, **185**, no. 1, 539–556.

Pratt, R. G., 1999, Seismic waveform inversion in the frequency domain, Part I: Theory and verification in a physic scale model: Geophysics, **64**, 888–901, doi:10.1190/1.1444597.

Pratt, G., C. Shin, and G. J. Hicks, 1998, Gauss-Newton and full Newton methods in frequency-space seismic waveform inversion: Geophysical Journal International, **133**, no. 2, 341–362, doi:10.1046/j.1365-246X.1998.00498.x.

Pratt, G., and M. H. Worthington, 1990, Inverse theory applied to multisource cross-hole tomography, Part I: Acoustic waveequation method: Geophysical Prospecting, **38**, no. 3, 287–310, doi:10.1111/j.1365-2478.1990.tb01846.x.

Prieux, V., S. Operto, R. Brossier, J. Virieux, J. Kommendal, and O. Barkved, 2010, Application of 2D acoustic frequency-domain full-waveform inversion to OBC wide-aperture data from the Valhall Field: 80th Annual International Meeting, SEG, Expanded Abstracts, **29**, 920–924, doi:10.1190/1.3513928.

Ravaut, C., S. Operto, L. Improta, J. Virieux, A. Herrero, and P. dell'Aversana, 2004, Multiscale imaging of complex structures from multifold wide-aperture seismic data by frequency-domain full-

waveform tomography: Application to a thrust belt: Geophysical Journal International, **159**, no. 3, 1032–1056, doi:10.1111/j.1365-246X.2004.02442.x.

Sirgue, L., O. I. Barkved, J. Dellinger, J. Etgen, U. Albertin, and J. H. Kommedal, 2010, Full-waveform inversion: the next leap forward in imaging at Valhall: First Break, **28**, 65–70.

Sirgue, L., and R. G. Pratt, 2004, Efficient waveform inversion and imaging: a strategy for selecting temporal frequencies: Geophysics, **69**, 231–248, doi:10.1190/1.1649391.

Tarantola, A., 1986, A strategy for nonlinear elastic inversion of seismic reflection data: Geophysics, **51**, 1893–1903, doi:10.1190/1.1442046.

Thomsen, L. A., 1986, Weak elastic anisotropy: Geophysics, **51**, 1954–1966, doi:10.1190/1.1442051.

Virieux, J., and S. Operto, 2009, An overview of full waveform inversion in exploration geophysics: Geophysics, **74**, no. 6, WCC1–WCC26, doi:10.1190/1.3238367.